

# Three-dimensional medial shape representation incorporating object variability

Martin Styner

Guido Gerig

Department of Computer Science  
University of North Carolina  
Chapel Hill, NC 27514

## Abstract

*This paper presents a novel processing scheme for the automatic computation of a medial shape model which is representative for an object population with shape variability. The sensitivity of medial descriptions to object variations and small boundary perturbations are fundamental problems of any skeletonization technique. These problems are approached with the computation of a model with common medial branching topology and grid sampling. This model is then used for a medial shape description of individual objects via a constrained model fit.*

*The process starts from parametric 3D boundary representations with existing point-to-point homology between objects. The Voronoi diagram of each sampled object boundary is grouped into medial sheets and simplified by a pruning algorithm using a volumetric contribution criterion. Medial sheets are combined to form a common medial branching topology. Finally, the medial sheets are sampled and represented as meshes of medial primitives.*

*We present new results on populations of up to 184 biological objects. For these objects the common medial branching topology is described by a small number of sheets. Despite the coarse medial sampling, a close approximation of individual objects is achieved.*

## 1. Introduction

Representation and analysis of shape is considered a difficult and challenging problem in computer vision and image analysis. Main motivations for shape characterization in vision are extraction of characteristic features for object recognition and retrieval in image databases, building shape models for model-based segmentation, and object tracking for navigation and surveillance. This paper specifically addresses shape representation of 3D objects, for example anatomical objects extracted from 3D medical image data. In contrast to most other research studies on object shape modeling, a major emphasis herein is put on objects expressing shape variability and on representations appropriate

for shape discrimination and statistical shape analysis of group differences.

Research on methods for representing shape can be broadly categorized into the following categories where shape is defined by a) corresponding landmarks and space warp with interpolation [1], b) a high-dimensional warping between image data and applying the deformation to a segmented object template [2, 3], c) a parameterization of object surfaces [4], d) an extraction of characteristic surface features [5], and e) an extraction of the medial axis and a graph description [6, 7, 8]. This paper focuses on the latter and discusses a new approach for 3D medial shape representation. A fundamental problem of any medial description is the sensitivity to boundary change. The boundary change sensitivity is approached in Voronoi skeletons by a simplification process called pruning that removes irrelevant branches of the Voronoi skeleton. Pruning methods most influential to our work have been developed by Naef [9] and Attali [10]. Golland's 2D skeletons [6] and Pizer's 3D m-rep description [8] are sampled medial models that are fitted to individual objects. Keeping the topology of the model fixed results in an implicit correspondence between objects. So far, the model has been built manually.

Tackling important open issues in 3D medial shape representation, we developed a new processing scheme for the computation of a sampled medial model that represents not only individual objects but a population of objects. The new modeling scheme includes the partition into individual skeletal sheets and a minimal sampling of each sheet, properties that were lacking so far but are essential for statistical shape analysis [11, 12].

This paper is organized as follows. We start with a general description of our scheme to compute the medial model. Then we discuss shape space, common medial branching topology and minimal sampling in detail. Next, the fit process of the medial model to individual objects is described. Finally we present applications to 3D brain structures.

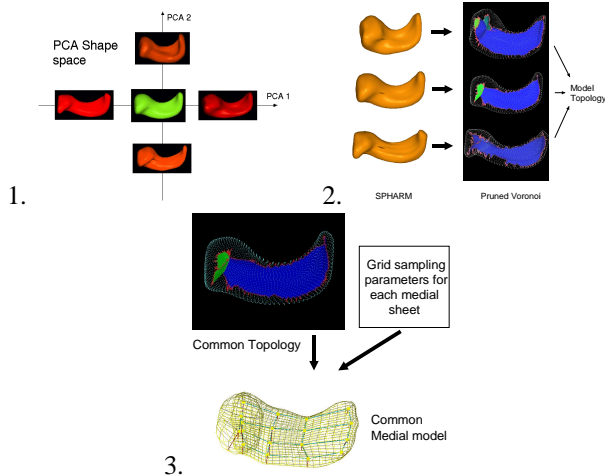


Figure 1: Computation of a m-rep model from an object population. 1. Shape space definition. 2. Common medial branching computation. 3. Minimal sampling computation.

## 2. Methods

The main problem addressed in this paper is: Given a population of similar objects, how can we automatically compute a stable medial model in the presence of shape variability? The following sections describe our scheme that constructs a medial *m-rep* model from an object population described by boundary parameterization using *spherical harmonics* (SPHARM) (see [13] for more details).

In overview, our scheme is divided into 3 steps and visualized in Fig. 1. We first define a shape space using Principal Component Analysis. From this shape space we generate the medial model in two steps. First we compute the common branching topology. Then we calculate the minimal sampling of the m-rep model given a maximal approximation error in the shape space.

### 2.1. M-rep and SPHARM shape description

**M-rep models.** A m-rep is a linked set of medial primitives [8] called medial atoms,  $m = (x, r, \underline{F}, \theta)$ . The atoms are formed from two equal length vectors and are composed of 1) a position  $x$ , 2) a width  $r$ , 3) a frame  $\underline{F} = (\vec{n}, \vec{b}, \vec{b}^\perp)$  implying the tangent plane to the medial manifold and 4) an object angle  $\theta$ . The medial atoms are grouped into figures connected via inter-figural links. These figures are defined as unbranching medial sheets and together form the medial branching topology. A figure is formed by a set of medial atoms connected by intra-figural links. The connections between primitives form a graph called 'medial graph' with edges representing either inter- or intra-figural links.

**SPHARM** The SPHARM description is a parametric surface description that can only represent objects of spherical topology [4]. The basis functions of the parameterized surface are spherical harmonics. Kelemen [14] demonstrated that SPHARM can be used to express shape deformations.

SPHARM is a smooth, accurate fine-scale shape representation, given a sufficiently small approximation error. Based on a uniform icosahedron-subdivision of the spherical parameterization, we obtain a Point Distribution Model (PDM) directly from the coefficients via a linear mapping. Correspondence of SPHARM is determined by normalizing the parameterization to the first order ellipsoid.

### 2.2. Shape space via PCA

As a first step in our scheme, we compute a shape space using Principal Component Analysis (PCA) of parametrized objects from a training population. The shape space smoothes the shape variability in the training population, thus making the computations of our scheme more stable. We assume that the shape space is an appropriate representation of the object's biological variability. PCA is applied to SPHARM objects  $\vec{c}_i$  of the training population as described by Kelemen [14]. The PCA results in an average coefficient vector  $\vec{c}$  and the eigenmodes of deformation  $\{(\lambda_1, \vec{v}_1) \dots (\lambda_{n-1}, \vec{v}_{n-1})\}$ . The first  $k$  eigenmodes  $\{(\lambda_1, \vec{v}_1) \dots (\lambda_k, \vec{v}_k)\}$  are chosen to cover at least 95% of the population's variability.

A discrete description of the shape space is gained by sampling it either uniformly or probabilistically. These samples form an object set that is a representative sampling of the shape space. All subsequent computations of the model building are then applied to this object set.

### 2.3. Common medial branching topology

This section describes the computation of the common medial branching topology. First we compute for each object in the shape space its branching topology as a set of medial sheets using Voronoi skeletons. Then we establish a common spatial frame in order to compare the topology of different objects. Finally we determine the common branching topology via a spatial matching in the common frame.

**Medial branching topology of a single object.** The branching topology of an individual object is represented by a set of medial sheets from the pruned Voronoi skeleton. We first calculate a finely sampled PDM from the object described by SPHARM. The inner 3D Voronoi diagram is then calculated from the PDM. This 'raw' Voronoi skeleton is very complex so that a pruning process is needed to simplify the skeleton.

Our pruning scheme starts with grouping the Voronoi skeleton into a set of non-branching, non-self-intersecting medial sheets. The grouping algorithm is based on the graph-algorithm proposed originally by Näf [9]. Our extended version uses a cost function weighted by a geometric continuity criterion. Additionally, a merging step has been implemented, which merges similar sheets according to a mixed radial and geometric continuity criterion. The pruning scheme treats the medial sheets as independent of each

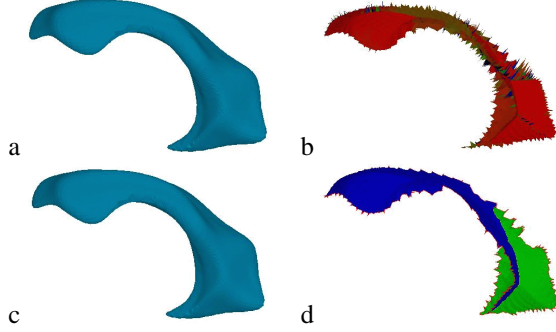


Figure 2: Voronoi skeleton pruning scheme applied to a lateral ventricle (side views). a. Original boundary. b. Original Voronoi skeleton ( $\sim 1600$  sheets). c. Reconstructed boundary from pruned skeleton ( $E_{\text{overlap}} = 98.3\%$ ). d. Pruned skeleton (2 sheets).

other. A simple thresholding of the significance criterions described below marks the sheets that are to be pruned. The medial sheets are then pruned using a topology preserving deletion scheme.

The pruning of medial sheets usually changes the branching topology of the skeleton by creating new sheets or by merging existing sheets. Therefore, a sheet-based pruning scheme has to include an additional grouping step that is performed directly after the pruning step if any sheet was pruned. Then, the skeleton needs to be pruned again with the same criterion, which possibly changes the branching topology again. Thus, the sheet-pruning scheme applies a loop consisting of a grouping step followed by pruning step until no sheet can be pruned.

The global significance criterion we propose uses the volumetric contribution of the reconstruction to the object:  $C_{\text{volume}} = V_{\text{skel}} - V_{\text{skel}-s_i} / V_{\text{skel}}$ . This volumetric contribution criterion correlates directly with the significance of a sheet to the object shape. However, the volumetric contribution criterion is computationally inefficient and thus as a first step, the pruning scheme removes tiny medial sheets from the skeleton. Fig. 2 shows the result of the pruning scheme applied to a real object.

Our experiments show that a considerable reduction of the number of medial sheets is possible with sacrificing only little accuracy of the reconstruction. In fact, the pruned skeletons of *all* objects studied so far had a volumetric overlap with the original object of more than 98%.

**A common spatial frame for branching topology comparison.** The problem of comparing branching topologies has already been addressed before in 2D by Siddiqi [7] and others, mainly via matching medial graphs. To our knowledge, there has been no work reported in 3D to date. August [15] showed that the medial branching topology is quite unstable. Thus, we developed a matching algorithm that is not based on graph matching but on spatial correspondence.

The branching topology is thereby represented by the spatial distributions of medial sheets.

All objects to be compared are mapped into a common spatial frame by a warped registration (see Fig. 3). In order to minimize the mapping distortions, the average object of the shape space is chosen to provide the common spatial frame. The SPHARM description and its implied PDM are used to create correspondences on the boundary between each object and the template object in the common frame. The correspondence in the whole 3D space is interpolated from the PDM boundary correspondence via thin plate splines (TPS). The TPS-warp maps every skeleton into the common frame, where the PDM's match perfectly.

**Extraction of a common branching topology.** Given that all medial sheets of the object set are mapped into a common spatial frame, a matching criterion can be defined to assess how well two different sheets spatially correspond. Visually, a high degree of overlap between matching sheets in the common frame can be observed. The centers of the medial sheets match better than the edges, which are quite sensitive to boundary noise. We developed a robust matching criterion that takes into account the non-isotropic spatial distribution of the Voronoi vertices of the medial sheets. Specifically, for every sheet  $s_i$  the covariance matrix  $\Sigma_i$  of its vertices and the average vertices' locations  $\mu_i$  (sheet center) are computed. This covariance matrix  $\Sigma_i$  can be seen as an ellipsoid approximating the spatial extension of the medial sheet  $s_i$ . The matching criterion is then computed as the paired Mahalanobis distance between the sheet centers:

$$d_{\text{Maha}}(s_i, x) = (x - \mu_i)' \cdot \Sigma_i^{-1} \cdot (x - \mu_i) \quad (1)$$

$$\text{crit}_{\text{Maha}}(s_i, s_j) = \frac{d_{\text{Maha}}(s_i, \mu_j) + d_{\text{Maha}}(s_j, \mu_i)}{2}$$

An empirically determined threshold leads to the rejection of a match if the sheet centers are further away than twice the paired Mahalanobis distance. This empirical threshold produced good results with the datasets studied so far, but it might need adaption for objects of different complexity.

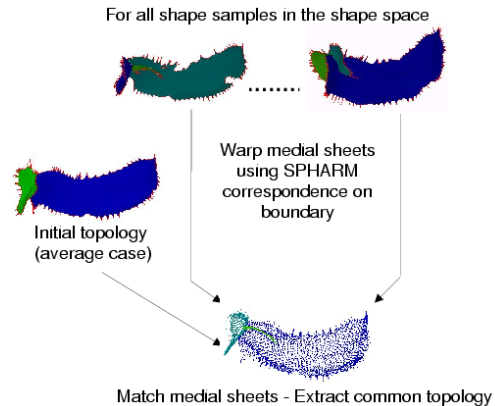


Figure 3: Schematic overview of matching procedure

The common branching topology is computed stepwise. First, the topology of the average object is chosen as the initial guess for the common branching topology. Step by step the algorithm chooses a different object of the shape space and compares its branching topology with the current common branching topology until the object set is fully processed. Those sheets that do not correspond to any sheet in the current common branching topology are added to it. This means that every sheet of the whole object set is matched by at least one of the sheets of the final common branching topology. The common branching topology is a set of medial sheets originating from various objects of the shape space mapped into the common spatial frame.

## 2.4. Minimal medial sampling

An m-rep model is determined by a set of medial sheets and the set of corresponding grid parameters  $\{n_i, m_i\}$ . In the next section, we describe the algorithm to compute the grid sampling of a single medial sheet given the sheet’s parameters  $n_i, m_i$ . This sampling algorithm is applied to all medial sheets in the common branching topology to compute the m-rep model. Next, we describe how this sampling algorithm is used to compute the minimal medial sampling in the shape space given a maximal approximation error.

**Sampling of a single medial sheet.** Given a medial sheet from the Voronoi skeleton and a set of m-rep grid dimensions  $n, m$ , how can we determine the grid samples for a most uniform grid on the medial sheet? The procedure proposed here computes this sampling on the volumetric reconstruction from the medial manifold rather than on the Voronoi skeleton since efficient and well-tested algorithms exist for a wide range of image operations.

The procedure first smoothes the voxel sampling of the medial sheet at its boundary. From the smoothed sheet, we compute the 1D skeleton using a 3D thinning procedure. After graph-compilation, the longest path is extracted from the thinning-skeleton to form the medial axis of the sheet. This axis is uniformly sampled. Next, the m-rep grid samples on the grid-edge are computed as the closest sheet boundary points of estimated locations along directions normal to the medial axis. Finally, the remaining grid samples are linearly interpolated along the lines connecting medial axis samples and grid-edge samples (see Fig. 4).

Since the computed medial samples do not lie at the locations of the Voronoi vertices, they are bijectively projected to the closest Voronoi vertices of the medial sheet. Since the medial manifold is densely sampled with Voronoi vertices, this projection affects the sample locations only slightly. At the Voronoi vertices, the additional information from the generating points and the Voronoi neighborhood is used to estimate the m-rep atom properties.

The computed m-rep is a good *initial* estimate to the m-rep description. An additional step computes the appropri-

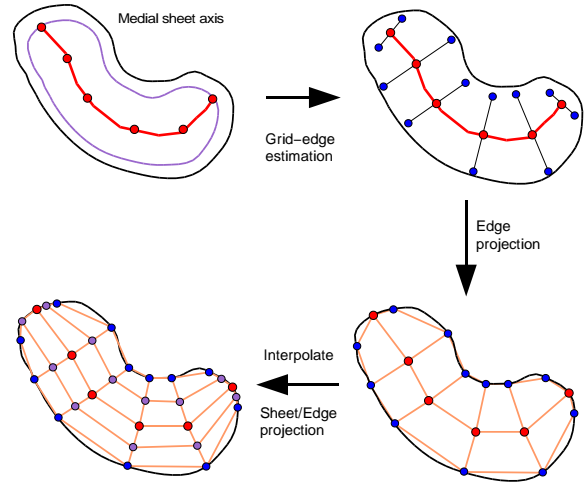


Figure 4: Visualization of the sampling method. Starting from the sampled axis (top left, boundary in black, eroded boundary in purple, axis in red), the grid-edge (top right, blue) is estimated. The grid-edge is projected to the sheet boundary (bottom right) and the remaining samples (violet) are interpolated.

ate m-rep description via deformation to optimally fit the object boundary (see section 2.5).

**Minimal sampling in shape space.** The grid dimensions  $\{n_i, m_i\}$  are optimized (nonlinear 1+1 evolutionary scheme) to be minimal while the m-rep model has a maximal approximation error in the shape space. The approximation error is defined as the Mean Absolute Distance (*MAD*) of the m-rep implied boundary and the original boundary. The proposed error  $E_{pop}$  is the *MAD* normalized using 2 the average radius over all skeletons of the population  $r_{avg}$ :  $E_{pop} = \frac{MAD}{r_{avg}}$ .

The next step computes the minimal sampling in the shape space. First, the m-rep model of the minimal sampling for the average object is computed as described above. Next, this m-rep model is checked whether it appropriately fits into all objects from the object set. If an object  $o_i$  of the object set has a larger  $E_{pop}$  than  $E_{max}$ , the current m-rep model is not appropriate for the whole shape space and has to be adjusted. In this case, the algorithm computes a new m-rep model with a minimal sampling for that object  $o_i$ . This m-rep model becomes the current m-rep model, which has to be checked to appropriately fit the whole object set. After all objects of the shape space have been handled by the algorithm, the resulting m-rep model represents the common m-rep model sought.

## 2.5. Fitting an m-rep model to an object

Once a common m-rep model is computed, it is used to describe individual objects via fitting the model into the ob-

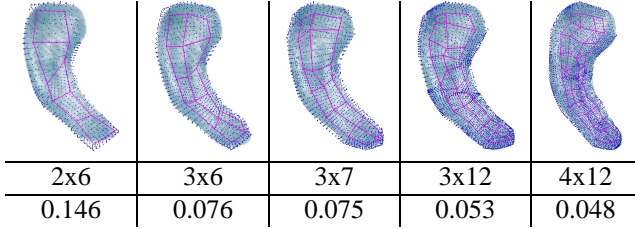


Figure 5: Sampling approximation errors  $E_{pop}$  of the m-rep implied surface (dark blue dots) with the original object boundary (light blue transparent) in a hippocampus structure ( $r_{avg} = 2.67$  mm). The m-rep grids are visualized as red lines. The grid dimensions are shown in the second row, and the  $E_{pop}$  errors in the third row.

ject boundaries. This fit process is done in 2 steps. First a good initial estimate is obtained, which is then refined in an optimization step. The initial estimate is computed by a TPS warp of the m-rep model from the common frame into the frame of the individual object using the SPHARM correspondence on the boundary. Starting from this initial position, an optimization procedure changes the properties of the m-rep model to improve the fit to the boundary [16]. Local similarity transformations as well as rotations of the local angulation are applied to the m-rep atoms.

### 3. Results

The scheme has been applied to different studies with populations of several human brain structures; the overall number of processed cases is shown in parenthesis: hippocampus-amygdala (60 cases), hippocampus (180), thalamus (56), pallide globe (56), putamen (56) and lateral ventricles (40). Fig. 6 presents a selection of the computed models. Two of the studies are presented in more detail in the following paragraphs.

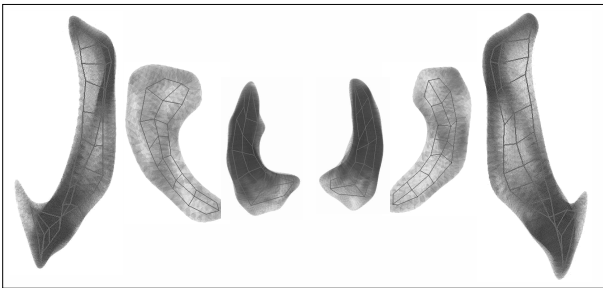


Figure 6: Selection of medial models of anatomical structures in the left and right brain hemisphere. From outside to inside: lateral ventricle, hippocampus, pallide globe.

**Hippocampus schizophrenia study.** The hippocampus structure of an object population with schizophrenic patients (56 cases) and healthy controls (26 cases) is investigated. One goal of the study was to assess shape asymmetry between left and right side objects. The model was built on

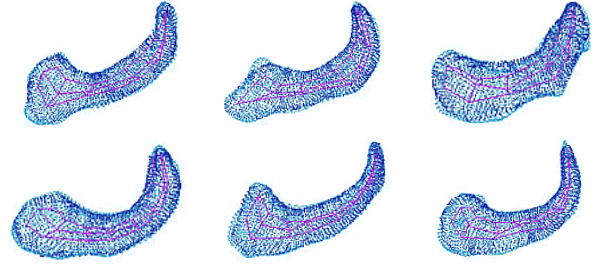


Figure 7: Six individual m-rep descriptions of the hippocampus study. The visualizations show m-rep grids as red lines, the m-rep implied surface as dark blue dots and the original object boundary in transparent light blue.

a object population that included the objects of all subjects on both sides, with the right hippocampi mirrored at the interhemispheric plane.

The SPHARM coefficients were normalized for rotation and translation using the first order ellipsoid. The size was normalized to unit volume. The shape space was defined by the first 13 eigenmodes with every other eigenmode holding less than 1% of the variability in the population. All objects in the shape space had a medial branching topology of a single medial sheet with a volumetric overlap of more than 98%. Thus, the common topology was a single sheet. The computed minimal grid sampling of 3x8 had an  $E_{pop}$  error of less than 5% for all objects in the shape space. The application to the whole hippocampus population of 164 objects generated  $E_{pop}$  errors in the range of [0.048 . . . 0.088] with an average error of 0.058. The average radius is 3.0 mm and thus the average error is 0.17mm. Some m-rep objects are shown in Fig. 7.

**Lateral ventricle twin study.** Another study investigates the lateral ventricle structure in an object population with 10 mono- and 10 di-zygotic twins. The same processing has been performed as in the first case.

The SPHARM coefficients were normalized for rotation and translation using the first order ellipsoid. The size was normalized to unit volume. The first 8 eigenmodes define the shape space, which holds 96% of the variability of the population. The medial branching topologies varied between one to three medial sheets with a volumetric overlap of more than 98% for each object. The single medial sheet topology of the average object matched all sheets in the common frame. Thus, the common medial topology was computed to be a single sheet. The minimal sampling of the medial topology was computed with a maximal  $E_{pop} \leq 0.10$  in the shape space. The application to the whole population generated  $E_{pop}$  errors in the range of [0.057 . . . 0.15] with an average error of 0.094. The average radius is 2.26mm and thus the average error is 0.21mm. Some m-rep objects are shown in Fig. 8.

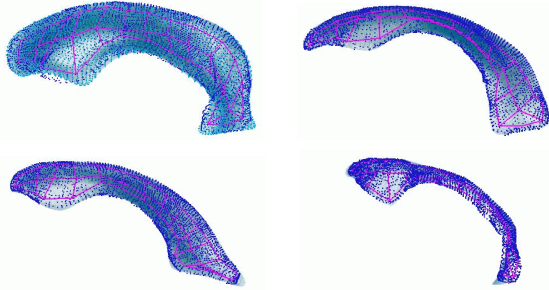


Figure 8: Four individual m-rep descriptions of the lateral ventricle study. The visualizations show m-rep grids as red lines, the m-rep implied surface as dark blue dots and the original object boundary in transparent light blue.

## 4. Summary and Conclusions

This paper presents a new processing scheme for medial shape representation with following novel features: The medial model represents the common branching topology of a range of objects characterized by a predefined shape space. Voronoi skeletons with only a small set of medial sheets are obtained by an improved grouping and pruning method. Point to point correspondence between medial sheets, a property most essential for building statistical shape models and for shape comparison, is achieved by calculating skeletons from a parametrized surface description with existing correspondence. The dense sampling of the Voronoi skeleton is replaced by a discrete grid with optimal sampling given the degree of approximation. Sensitivity to boundary changes resulting in instability of skeleton edges and branching locations are tackled by starting from smooth parametrized object surfaces and by developing new techniques for combination of the medial sheet topology of similar objects and calculation of an optimal grid sampling.

The results of processing large series of objects clearly demonstrate the feasibility of a medial representation even with only a few sheets to capture coarse-scale shape of a whole shape population. Shape models calculated by the scheme presented herein will be used for model-based segmentation and for the detection of group differences between patients and controls. In contrast to surface-based object representation, a medial representation captures growth and bending independently, a property most desirable for shape description. Further, it provides type and magnitude of shape changes with locality. Both properties make it the shape representation of our choice for studying biological objects, for example for studying neuro-development and neuro-degeneration in brain research.

## Acknowledgments

M. Chakos and the MHNCR image analysis lab at UNC Psychiatry kindly provided the hippocampi original MR and segmentations. We acknowledge D. Weinberger, NIMH

Neuroscience in Bethesda for providing the twin datasets. We are thankful to C. Brechbühler for providing the SPHARM software. We are further thankful to S. Pizer and S. Joshi of the MIDAG group at UNC for providing the m-rep tools and for comments and discussions about m-rep and other medial descriptions.

## References

- [1] F.L. Bookstein, "Shape and the Information in Medical Images: A Decade of the Morphometric Synthesis," *Comp. Vision and Image Under.*, vol. 66, no. 2, pp. 97–118, May 1997.
- [2] C. Davatzikos, M. Vaillant, S. Resnick, J.L. Prince, S. Letovsky, and R.N. Bryan, "A computerized method for morphological analysis of the corpus callosum," *J. of Comp. Ass. Tomography.*, vol. 20, pp. 88–97, Jan./Feb 1996.
- [3] S. Joshi, M. Miller, and U. Grenander, "On the geometry and shape of brain sub-manifolds," *Pattern Recognition and Artificial Intelligence*, vol. 11, pp. 1317–1343, 1997.
- [4] C. Brechbühler, *Description and Analysis of 3-D Shapes by Parametrization of Closed Surfaces*, 1995, Diss., IKT/BIWI, ETH Zürich, ISBN 3-89649-007-9.
- [5] G. Subsol, J.P. Thirion, and N. Ayache, "A scheme for automatically building three-dimensional morphometric anatomical atlases: application to a skull atlas," *Med. Image Analysis*, vol. 2, no. 1, pp. 37–60, 1998.
- [6] P. Golland, W.E.L. Grimson, and R. Kikinis, "Statistical shape analysis using fixed topology skeletons: Corpus callosum study," in *Inf. Proc. in Med. Imaging*, 1999, pp. 382–388.
- [7] K. Siddiqi, A. Ahokoufandeh, S. Dickinson, and S. Zucker, "Shock graphs and shape matching," *Int. J. Computer Vision*, vol. 1, no. 35, pp. 13–32, 1999.
- [8] S. Pizer, D. Fritsch, P. Yushkevich, V. Johnson, and E. Chaney, "Segmentation, registration, and measurement of shape variation via image object shape," *IEEE Trans. Med. Imaging*, vol. 18, pp. 851–865, Oct. 1999.
- [9] M. Näf, *Voronoi Skeletons: a semicontinuous implementation of the 'Symmetric Axis Transform' in 3D space*, Ph.D. thesis, ETH Zürich, Communication Technology Institute IKT/BIWI, 1996.
- [10] D. Attali, G. Sanniti di Baja, and E. Thiel, "Skeleton simplification through non significant branch removal," *Image Proc. and Comm.*, vol. 3, no. 3-4, pp. 63–72, 1997.
- [11] M. Styner and G. Gerig, "Medial models incorporating shape variability," in *Inf. Proc. in Med. Imaging*, 2001, pp. 502–516.
- [12] G. Gerig and M. Styner, "Shape versus size: Improved understanding of the morphology of brain structures," in *Med. Image Comp. and Comp.-Ass. Intervention*, 2001, accepted for publication.
- [13] Martin Styner, *Combined Boundary-Medial Shape Description of Variable Biological Objects*, Ph.D. thesis, UNC Chapel Hill, Computer Science, June 2001, available at [www.ia.unc.edu/public/styner/docs/diss.html](http://www.ia.unc.edu/public/styner/docs/diss.html).
- [14] A. Kelemen, G. Székely, and G. Gerig, "Elastic model-based segmentation of 3d neuroradiological data sets," *IEEE Trans. Med. Imaging*, vol. 18, pp. 828–839, October 1999.
- [15] J. August, K. Siddiqi, and S. Zucker, "Ligature instabilities in the perceptual organization of shape," in *IEEE Comp. Vision and Pattern Rec.*, 1999.
- [16] S. Joshi, S. Pizer, T. Fletcher, A. Thall, and G. Tracton, "Multi-scale deformable model segmentation based on medial description," in *Inf. Proc. in Med. Imaging*, 2001.